Second-harmonic generation from a positive-negative index material heterostructure

Nadia Mattiucci,[1,2] Giuseppe D'Aguanno,[1] Mark J. Bloemer,[3] and Michael Scalora[3]
[1]*Time Domain Corp., Cummings Research Park, 7057 Old Madison Pike, Huntsville, Alabama 35806, USA*
[2]*Universita' "RomaTre" Dipartimento di Fisica "E. Amaldi," Via Della Vasca Navale 84, 1-00146 Rome, Italy*
[3]*Charles M. Bowden Research Facility, Bldg. 7804, US Army Research, Development, and Engineering Command, Redstone Arsenal, Alabama 35898-5000, USA*
(Received 9 August 2005; published 21 December 2005)

Resonant cavities have been widely used in the past to enhance material, nonlinear response. Traditional mirrors include metallic films and distributed Bragg reflectors. In this paper we propose negative index material mirrors as a third alternative. With the help of a rigorous Green function approach, we investigate second harmonic generation from single and coupled cavities, and theoretically prove that negative index material mirrors can raise the nonlinear conversion efficiency of a bulk material by at least four orders of magnitude compared to a bulk medium.

DOI: 10.1103/PhysRevE.72.066612 PACS number(s): 42.70.Qs, 42.65.Ky

I. INTRODUCTION

An optical cavity is a region bounded by two or more mirrors. In a resonant cavity, the mirrors are aligned to improve light confinement inside the cavity at a certain frequency or range of frequencies. The efficiency of the cavity depends on the characteristics of the mirrors. Traditional mirrors may use metallic mirrors (MM) and/or distributed Bragg reflectors (DBR). MMs exhibit high reflectivity over a broad spectral range. Unfortunately, they are limited by absorptive losses, and are not suitable for transmission-type devices. Moreover, cavities made with MMs are not frequency selective, i.e., cavity resonances are quite broad and field localization remains low. DBRs are multilayer dielectric mirrors. They have low losses, but to achieve high reflectivity high precision in layer thicknesses and refractive indices are required. The distributed nature of the reflection sharpens the cavity resonances: a DBR cavity exhibits resonances that are typically much narrower compared to the same cavity made using MMs. Perhaps more importantly, field localization and enhancement inside DBR cavities can be several orders of magnitude greater compared to equivalent MMs cavities. Therefore, while a DBR cavity may be much more efficient than a MMs cavity, they require a more careful design with restricted range of frequencies.

In this paper we will study the characteristic of negative index materials (NIMs) mirrors. NIMs are materials that display negative electric and magnetic susceptibility simultaneously, and that refract light in the opposite way with respect to what an ordinary material does. During the past five years, NIMs have been the subject of intense theoretical and experimental investigations [1–3]. In 2001 Shelby, Smith, and Schultz published the results of an experiment that confirmed negative refraction in the microwave regime [1]. Arguably, the most important result contained in Ref. [1] was the demonstration that NIMs in fact do exist in the form of man-made artificial materials that can be assembled and engineered. The results of Ref. [1], taken together with the pioneering work of Veselago in the late 1960s [2] and the studies conducted by Pendry on NIM lenses [3], have opened a new field of research.

According to the experimental results reported in Ref. [1], one can reasonably simulate the electric and magnetic responses of a NIM by using a lossy Drude model [3–9]. As shown in Refs. [6–8], a single slab of NIM manifests an intrinsic gap in the transmission spectrum in the region located between the electric (ω_{pe}) and magnetic (ω_{pm}) plasma frequency. This intrinsic gap is surrounded by a pass band with transmission resonances that resemble the transmission resonances near the band edges of one-dimensional photonic band gap structures (PBGs) [6]. The spectral region that comprehends the intrinsic gap and the pass band displays some interesting properties, for example: the possibility of exciting dark and bright gap solitons [7], the possibility to fabricate an efficient hollow waveguide [8], the presence of a zero group velocity dispersion point [9].

In this work our aim is to study second harmonic generation in single and coupled cavities made of a generic, quadratic, positive index material (PIM) sandwiched between two negative index materials. Some of the linear and nonlinear properties of NIM/PIM cavities have been already studied: for example, in Ref. [10] a PIM/NIM/PIM structure is studied; Ref. [11] deals with finite and infinite one-dimensional photonic crystals (1-D PCs) made of a NIM/PIM unit cell; in Refs. [12,13] omni-directional reflectance is predicted for NIM/PIM 1-D PCs; finally, in Ref. [14], the authors show how an optical diode can be realized with NIM/PIM stratifications. Our work differs from the works cited above in that we focus on the region where the NIM displays its intrinsic gap, where the refractive index is approximately equal to zero as its magnitude changes sign, as discussed at length in Ref. [8].

II. SINGLE CAVITY

We begin by studying the linear and nonlinear behavior of a single NIM/PIM/NIM cavity. The electric and magnetic responses of the NIM are modeled with a lossy Drude model [5]:

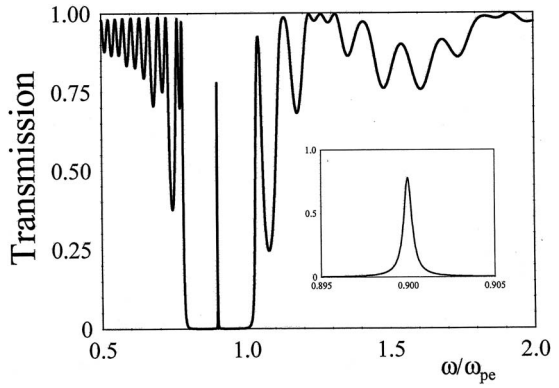

FIG. 1. Transmission spectrum of a NIM/PIM/NIM cavity vs ω/ω_{pe}. The thickness of each layer of NIM is $2.5\lambda_{pe}$, while the thickness of the PIM is $0.16338\lambda_{pe}$ and $\lambda_{pe}=2\pi c/\omega_{pe}$ is the electric plasma wavelength. The PIM is assumed to be nondispersive and nonabsorbing with a refractive index of $n=1.4$. Inset: magnification of the defect resonance inside the gap. The defect resonance is centered around $0.9\omega_{pe}$.

$$\varepsilon^{\mathrm{NIM}}(\tilde{\omega}) = 1 - \frac{1}{\tilde{\omega}(\tilde{\omega} + i\tilde{\gamma}_e)}, \quad \mu^{\mathrm{NIM}}(\tilde{\omega}) = 1 - \frac{(\omega_{pm}/\omega_{pe})^2}{\tilde{\omega}(\tilde{\omega} + i\tilde{\gamma}_m)}, \tag{1}$$

where $\tilde{\omega}=\omega/\omega_{pe}$ is the normalized frequency, ω_{pe} and ω_{pm} are the respective electric and magnetic plasma frequencies, and $\tilde{\gamma}_e=\gamma_e/\omega_{pe}$ and $\tilde{\gamma}_m=\gamma_m/\omega_{pe}$ are the respective electric and magnetic loss terms normalized with respect to the electric plasma frequency. Here we take $\omega_{pm}/\omega_{pe}=0.8$, and $\gamma_e/\omega_{pe}=\gamma_m/\omega_{pe}=10^{-4}$. As discussed at length in Refs. [6–8], the transmission spectrum of a single layer of NIM exhibits a gap with band-edge resonances around the electric and magnetic plasma frequencies that are very similar to those of a PBG structure. In our case, the gap of the single slab of NIM is located in the spectral range between $0.8<\tilde{\omega}<1$. Moreover, the width of the gap depends upon the separation of the electric and magnetic plasma frequencies, and its depth is related to the thickness of the layer [6]. Now, when we sandwich one layer of PIM between two layers of NIMs, a transmission resonance appears in the middle of the gap, similar to a defect-resonance of PBG structures. In Fig. 1 we plot the transmission spectrum of a cavity made with a single layer of nondispersive PIM enclosed between two layers of NIM. The layers of NIM have thicknesses $a=2.5\lambda_{pe}$, while the PIM layer has thickness $d=0.16338\lambda_{pe}$, where $\lambda_{pe}=2\pi c/\omega_{pe}$ is the electric plasma wavelength. The thickness of the PIM has been chosen in order to have a transmission resonance at the frequency $\tilde{\omega}=0.9$, and its refractive index is assumed to be $n=1.4$. Note that at $\tilde{\omega}=1.8$, or double the frequency where the transmission resonance occurs, the curve is relatively smooth. In Fig. 2(a) we choose $\tilde{\omega}=0.9$, and plot the transmission as a function of the PIM thickness. In Figs. 2(b) and 2(c) we show magnifications of the first and second transmission resonances, which correspond to PIM layer thicknesses of $d=0.16338\lambda_{pe}$ [Fig. 2(b)] and $d=0.5602\lambda_{pe}$ [Fig. 2(c)], respectively. In Figs. 3(a) and 3(b) we show field localization inside the structure corresponding to the first and the second transmission resonances shown in Fig. 2, respectively. As one may expect, the field intensity is single-peaked at the first transmission resonance, double-peaked at the second transmission resonance, and so on.

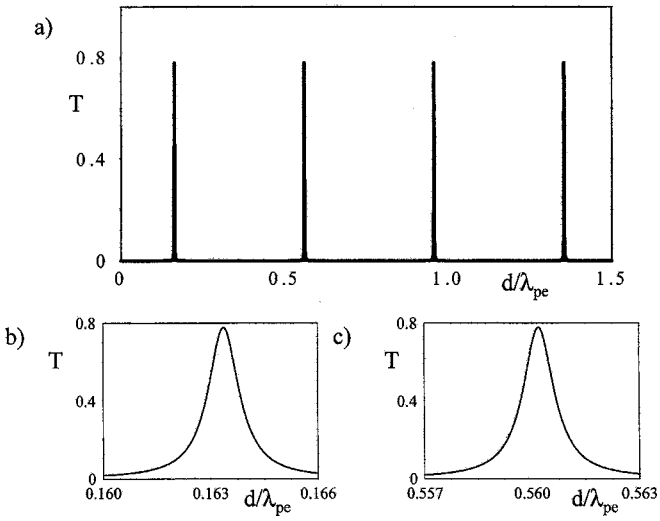

FIG. 2. (a) Transmission vs PIM thickness, for the NIM/PIM/NIM cavity described in Fig. 1 at the frequency of $0.9\omega_{pe}$ that corresponds to the peak of the band gap transmission resonance in Fig. 1. The thickness of the two NIM mirrors is fixed at $2.5\lambda_{pe}$. (b) Magnification of the first transmission resonance around $d=0.16338\lambda_{pe}$. (c) Magnification of the second transmission resonance around $d=0.5602\lambda_{pe}$.

Let us go to the main focus of our study, i.e., second harmonic generation (SHG) in this cavity where only the PIM possesses a quadratic nonlinearity. Under the monochromatic, plane wave approximation, and for normal incidence, the Helmholtz equations that describe SHG in the NIM/PIM/NIM cavity are given by

$$\frac{d^2E_\omega}{dz^2} + \frac{\omega^2\varepsilon_\omega(z)\mu_\omega(z)E_\omega}{c^2} = -2\frac{\omega^2}{c^2}\mu_\omega d^{(2)}(z)E_\omega^* E_{2\omega}, \tag{2a}$$

$$\frac{d^2E_{2\omega}}{dz^2} + \frac{(2\omega)^2\varepsilon_{2\omega}(z)\mu_{2\omega}(z)E_{2\omega}}{c^2} = -\frac{(2\omega)^2}{c^2}\mu_{2\omega}d^{(2)}(z)E_\omega^2, \tag{2b}$$

where $\varepsilon_{\omega,2\omega}$, $\mu_{\omega,2\omega}$ are, respectively, the z-dependent electric susceptibility and magnetic permeability at the fundamental (FF) and second harmonic (SH) frequency. $d^{(2)}$ is the quadratic coupling coefficient of the PIM: $\varepsilon_{\omega,2\omega}=\varepsilon^{\mathrm{NIM}}_{\omega,2\omega}$, $\mu_{\omega,2\omega}=\mu^{\mathrm{NIM}}_{\omega,2\omega}$, and $d^{(2)}=0$ for $0<z<a$ and $2a+d>z>a$; $\varepsilon_{\omega,2\omega}=\varepsilon^{\mathrm{PIM}}_{\omega,2\omega}$, $\mu_{\omega,2\omega}=1$, and $d^{(2)}\neq 0$ for $a<z<a+d$, where a and d are the thicknesses of the NIM and PIM layers, respectively, and $L=2a+d$ is the total length of the structure. In what follows we suppose that the structure is surrounded by air. Equations (2a) and (2b) should be solved in each layer separately and then the solutions should be matched at the interfaces by using the boundary conditions appropriate to the case of magnetically active materials. In general, given the nonlinear nature of the equations, this

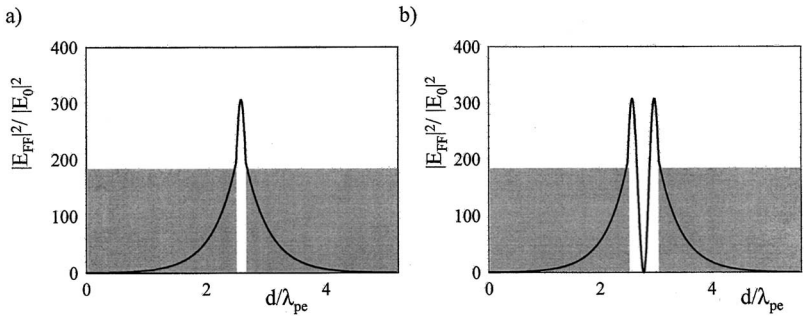

FIG. 3. Square modulus of the electric field for the NIM/PIM/NIM cavity at $0.9\omega_{pe}$ (a) when the PIM thickness is $0.16638\lambda_{pe}$ and (b) when the PIM thickness is $0.5602\lambda_{pe}$.

computational task can be accomplished only numerically. In the undepleted pump regime, a fast and elegant way to proceed is to resort to the Green function approach. In that case, the formal expression for the electric fields that is valid inside the structure can be written as

$$E_\omega(z) = A\Phi_\omega^+(z) + B\Phi_\omega^-(z), \tag{3a}$$

$$E_{2\omega}(z) = -4\frac{\omega^2}{c^2}\int_0^L G_{2\omega}(\xi,z)d^{(2)}(\xi)E_\omega^2(\xi)d\xi, \tag{3b}$$

where Φ_ω^+ and Φ_ω^- are the right-to-left (RTL) and left-to-right (LTR) linear modes of the structure at the FF as described in Refs. [15–17]. RTL and LTR propagating modes can be calculated independently using a standard linear matrix-transfer technique [18] adapted to the case of magnetic active materials. In Eq. (3a), A and B are complex coefficients that have the dimensions of an electric field. These coefficients are uniquely determined by the boundary conditions. In the special case of LTR incidence B is zero, while A is the complex amplitude of the FF pump field incident from LTR. In Eq. (3b), $G_{2\omega}$ is the Green function at frequency 2ω. The Green function can be calculated in terms of the RTL and LTR propagating modes of the structure at frequency 2ω. In order to do so, the theory developed in Refs. [16,17] has been extended to magnetically active media (see the Appendix for details).

Equation (3a) gives the generated electric SH field in all the space, and allows the calculation of the conversion efficiency (η). In the plane wave regime the conversion efficiency is defined as the sum of the forward and backward generated SH intensity divided by the input pump intensity:

$$\eta = \frac{I_{2\omega,\text{backward}}^{\text{output}} + I_{2\omega,\text{forward}}^{\text{output}}}{I_\omega^{\text{input}}}, \tag{4}$$

where $I_{2\omega,\text{backward}}^{\text{output}} = (1/2)\varepsilon_0 c|E_{2\omega}(0)|^2$ and $I_{2\omega,\text{forward}}^{\text{output}} = (1/2)\varepsilon_0 c|E_{2\omega}(L)|^2$ in the case of a cavity embedded in air, and I_ω^{input} is the intensity of the pump beam incident from LTR. Now, taking into account Eqs. (3a) and (4), and using Eqs. (A4) and (A5) of the Appendix, we finally arrive at an expression for the conversion efficiency in terms of overlap integrals [19]:

$$\eta = \frac{2\omega^2 L^2}{\varepsilon_0 c^3}\left(\left| \frac{1}{L}\int_0^L d^{(2)}(z)[\Phi_\omega^+(z)]^2\Phi_{2\omega}^-(z)dz \right|^2 + \left| \frac{1}{L}\int_0^L d^{(2)}(z)[\Phi_\omega^+(z)]^2\Phi_{2\omega}^+(z)dz \right|^2 \right) I_\omega^{\text{input}}. \tag{5}$$

In Eq. (5), two contributions to the conversion efficiency can be easily identified. The first integral refers to the forward conversion efficiency, while the second integral gives the backward conversion efficiency.

In Fig. 4(a) we plot the total conversion efficiency (forward+backward) as a function of the PIM thickness, when the pump is tuned to a frequency $\tilde{\omega}=0.9$, and its intensity is 100 MW/cm^2. The nonlinear coefficient is taken to be $d^{(2)}=9pm/V$. The conversion efficiency shows a series of

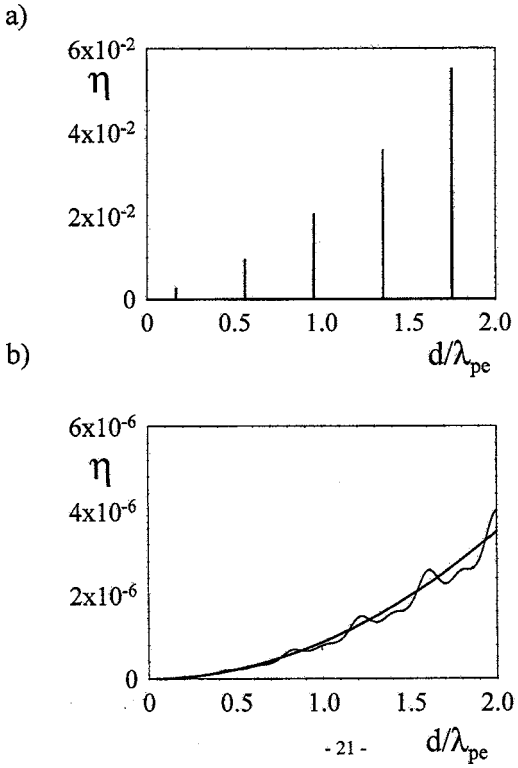

FIG. 4. (a) Conversion efficiency (η) vs PIM thickness for the NIM/PIM/NIM cavity. (b) Conversion efficiency vs thickness for a single layer of PIM. As explained in the text, the thin line refers to the conversion efficiency calculated considering the layer as a Fabry-Pérot etalon, the thick line considering it as a bulk material.

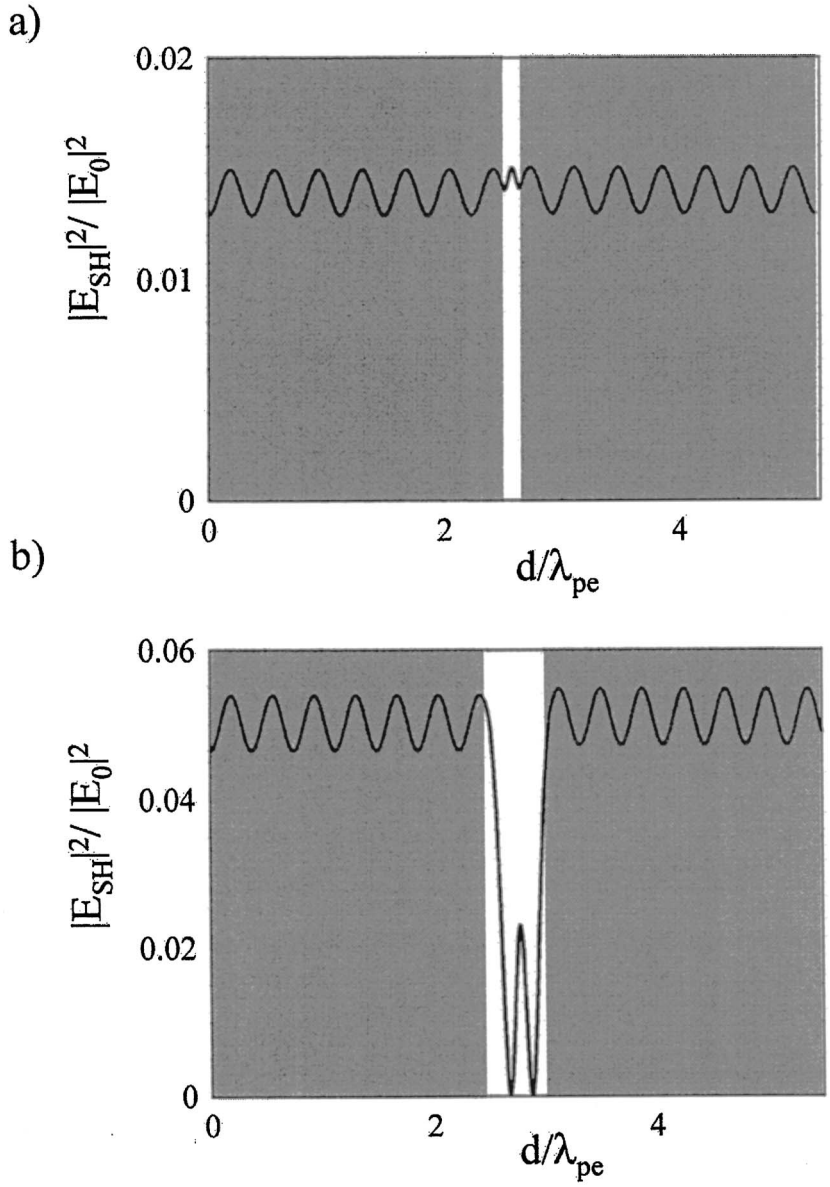

FIG. 5. Square modulus of the generated second harmonic electric field for (a) PIM thickness of $0.16638\lambda_{pe}$ and (b) PIM thickness is $0.5602\lambda_{pe}$. The pump field is tuned at $0.9\omega_{pe}$, i.e., at the transmission resonance in the band gap and its intensity is assumed to be 100 MW/cm^2. The quadratic nonlinearity of the PIM layer is $d^{(2)}=9$pm/V. The PIM is assumed to be nondispersive and nonabsorbing with a refractive index of 1.4.

peaks in correspondence to the transmission resonances shown in Fig. 2(a). In this case we have considered the quadratic material as being nondispersive. Note that the conversion efficiency grows approximately as the square of the length of the quadratic material, as one may expect for perfectly phase-matched interactions. For comparison, in Fig. 4(b) we plot the total conversion efficiency of a single layer of the same quadratic material as a function of its thickness. The conversion efficiency of the single layer has been calculated in two different ways: (a) considering it as a Fabry-Pérot etalon with all interference effects taken into account (thin line) and (b) considering it as a bulk material (thick line) using the standard formula for SHG in bulk materials [20]:

$$\eta = \frac{2\mu_0}{n_\omega^2 n_{2\omega} c}(d^{(2)}\omega L)^2 \frac{\sin^2(\Delta k d/2)}{(\Delta k d/2)^2} I_\omega^{\text{input}}, \tag{6}$$

where L is the length of the quadratic material, $\Delta k=(2\omega/c)\times(n_{2\omega}-n_\omega)$ is the phase mismatch, in the case of Fig. 4 $n_\omega=n_{2\omega}=1.4$, and I_ω^{input} is the input intensity calculated in a medium that has the same refractive index of the quadratic material at the FF frequency. The NIM/PIM/NIM cavity shows an enhancement in the conversion efficiency by a factor of 10^4 with respect to the PIM layer. Moreover, in the case of the NIM/PIM/NIM cavity the calculations shows that the SH signal is generated almost perfectly balanced in the forward and backward directions. Conversion efficiencies balanced in the forward and backward directions are typical of structures with high feedback, as discussed at length in Ref. [21] for the case of PBG structures. On the other hand, in the case of the single layer shown in Fig. 4(b), our calculations show that approximately 5% of the total conversion efficiency is generated in the backward direction. In Fig. 5 we plot the generated SH field for the first and the second resonance shown in Fig. 2.

Let us now investigate SHG outside of phase matching conditions. In Fig. 6(a) we plot the conversion efficiency of the NIM/PIM/NIM cavity as a function of the PIM thickness, and assuming a normal dispersion of 10% of the refractive

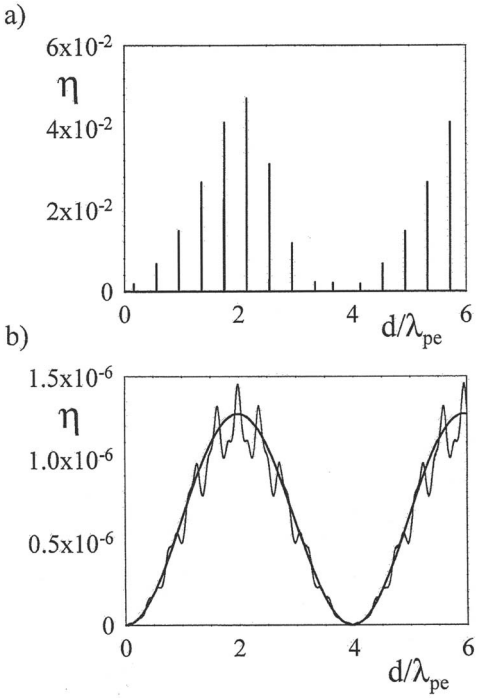

FIG. 6. (a) Conversion efficiency (η) vs PIM thickness as in Fig. 4(a) except that now the PIM is assumed to be dispersive with a 10% linear dispersion between the FF and the SH. (b) Conversion efficiency vs thickness for single layer of PIM. The thin and thick line refers, respectively, to the Fabry-Pérot and bulk configuration as in Fig. 5(b).

index of the PIM at the SH frequency with respect to the refractive index at the FF, i.e., $n_\omega=1.4$ and $n_{2\omega}=1.54$. In Fig. 6(b) we plot the conversion efficiency of a slab of the same PIM material as function of its thickness. As in Fig. 4, the thin line corresponds to the conversion efficiency calculated assuming the PIM layer is a Fabry-Pérot etalon, while the thick line is calculated using the bulk conversion efficiency Eq. (6). In this case the coherence length of the PIM calculated from Eq. (6) is $L_c=2\pi/\Delta k\cong 3.97\lambda_{pe}$. We note that the concept of coherence length is still valid in the case of the NIM/PIM/NIM cavity. In fact, comparing Figs. 6(a) and 6(b), it is evident that the conversion efficiency of the NIM/PIM/NIM cavity at the transmission resonances is approximately modulated by the function $\sin^2(\Delta kd/2)$. Comparing the SH energy generated from the NIM/PIM/NIM cavity to the SH generated in the single layer, our calculations show an enhancement factor of approximately 4×10^4. Once again we find that SH emission from the NIM/PIM/NIM cavity is balanced between the forward and backward directions, while in the single phase matched PIM layer SHG occurs almost completely in the forward direction. Finally, in Figs. 7(a) and 7(b) we plot the same quantities shown in Figs. 6(a) and 6(b), respectively, but now assuming a normal PIM dispersion of 20%. In this case the coherence length of the PIM calculated from Eq. (6) drops to $l_c=2\pi/\Delta k\cong 1.98\lambda_{pe}$, and the enhancement factor is approximately 4×10^4. One may therefore conclude that while material dispersion is detrimental to the conversion efficiency of the single PIM layer, the NIM/PIM/NIM cavity conversion efficiency seems to

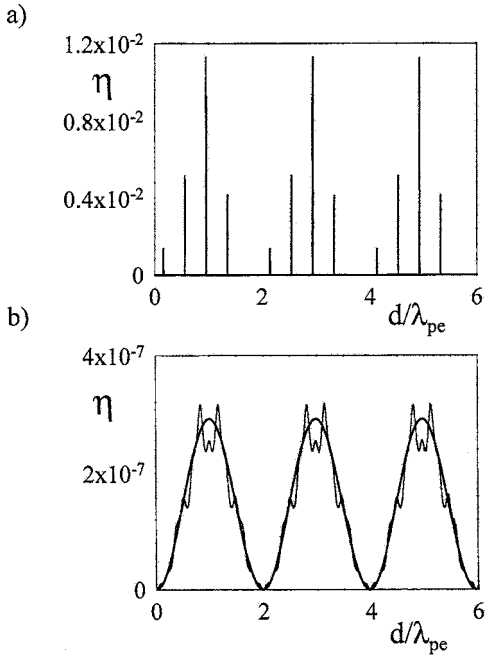

FIG. 7. Same as Fig. 6 except that now the PIM is assumed to have a 20% dispersion.

benefit by as much as a factor of 4 as the amount of dispersion changes from 10% to 20% (see Figs. 4, 6, and 7).

III. COUPLED CAVITIES

Let us now investigate the case of coupled, multiple cavities, and let us first discuss some of their linear properties. When we add more layers, the defect resonance found at the center of the gap splits into several transmission resonances whose number equals the number of coupled cavities, as one may expect. In Fig. 8 we show the transmission spectrum of a symmetric, 3 and 1/2 period structure, with initial and final NIM layers (Fig. 9). The thickness of each NIM layers is $a=2.5\lambda_{pe}$, and the thickness of each PIM layer is $d=0.5602\lambda_{pe}$. The PIM is assumed to be dispersive with a

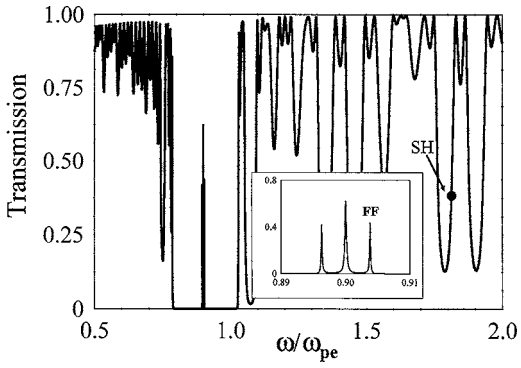

FIG. 8. Linear transmission of three coupled cavities, i.e., $(\mathrm{NIM/PIM})^3\mathrm{NIM}$ with a 20% dispersion in the PIM and PIM thickness $d=0.5602\lambda_{pe}$. The inset shows the three defect resonances that appear in the gap. The arrow indicates the tuning of the SH when the FF field is tuned at the third resonance.

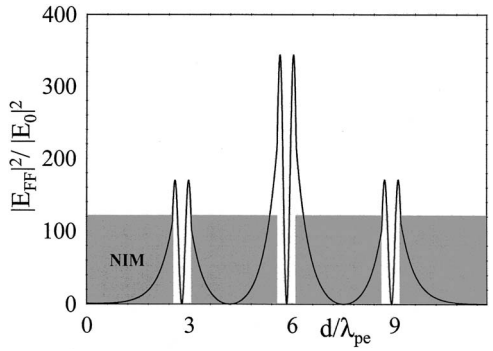

FIG. 9. Square modulus of the FF field when it is tuned at the third transmission resonance inside the band gap.

linear dispersion of 20% with respect to $\tilde{\omega}=0.9$, i.e., $n(\tilde{\omega})=1.4+(0.28/0.9)(\tilde{\omega}-0.9)$. The dispersion relations for the NIM layers are the same as those used for the single cavity. The inset of Fig. 8 shows the three defect resonances that appear inside the gap around $\tilde{\omega}=0.9$. Note that the spectral position of the gap does not depend on the number of coupled cavities. In fact, the gap remains positioned in the spectral region between the electric and magnetic plasma frequencies, as for the case of the single cavity (see Fig. 1). This fact confirms that the gap is intrinsic, i.e., it only depends on the dispersion relations of the NIM, not on any kind of interference effect from any of the layers, as it would for ordinary PBG structures made with PIMs [6–8], for example. Adding more cavities to the structure causes more transmission resonances to appear inside the gap, the transmission spectrum outside the gap become oscillates unpredictably, and SH emission is consequently much more difficult to control. For these reasons we focus our attention on the structure of Fig. 8, which is formed by only three coupled cavities. In Fig. 9 we plot the square modulus of the FF electric field tuned at the third transmission resonance inside the band gap of the structure. Note that the electric field profile inside the PIM layers is almost identical to the profile it has for the single cavity case [see Fig. 3(b)]. In Fig. 10 we plot the SH generated field when the FF is tuned to the third resonance peak. We find a conversion efficiency of 2.6% with an input pump of 100 MW/cm^2. We note that in the case of a single NIM/PIM/NIM cavity the maximum conversion efficiency available for the same intensity of input pump never exceeds 1.2% [see Fig. 7(a)]. We have also calculated the conversion efficiency when the pump is tuned to the first and the second transmission resonances. Tuning to the first transmission resonance yields a conversion efficiency of 1.3%, while tuning to the second resonance peak yields a conversion efficiency of 0.9%. The reasons the third resonance peak yields a higher conversion efficiency is due to a combination of higher field localization and better phase link for the FF and SH fields over the PIM layers; these conditions ultimately lead to a higher value of the square modulus of the overlap integrals calculated in Eq. (5).

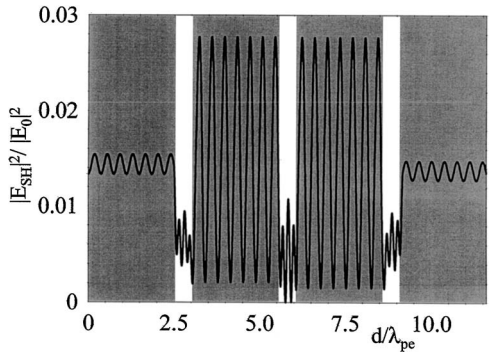

FIG. 10. Square modulus of the generated SH field for tuning conditions described in Fig. 8. The pump intensity and the quadratic nonlinearity of the PIM are the same used in the previous figures.

IV. CONCLUSIONS

In this paper we have explored the possibility of using NIMs as mirrors in the spectral region that contains an intrinsic gap, where the refractive index $n\cong 0$, in single or multiple coupled cavity configurations. In order to maximize SH generation from a resonant cavity, it is important that the cavity allow high field localization at both the fundamental frequency (FF) and the SH, and that the phases of the linear fields (light modes) interact constructively along the active area. In other words, the integrands of Eq. (5) must be maximized and must not change sign. MMs cavity are not efficient for SH generation, because field localization and enhancement is quite limited. In contrast, DBR cavities can significantly increase conversion efficiencies of SH and other nonlinear processes by several orders of magnitude, provided a more careful design process is followed to properly tune both FF and SH at narrow-band resonances. In comparison, NIM mirrors are a compromise solution between MMs and DBRs. In general, their efficiency is higher than the efficiency of MMs, but lower than that of DBRs. On the other hand, once a NIM with an intrinsic gap has been identified within the desired spectral range, the work is done. Recent advancements in the field of metamaterials suggest that NIMs operating in the near infrared regime (~ 1.5 μm) may be within reach [22–24], suggesting that NIM/PIM/NIM single and multiple cavities may be exploited to obtain efficient SHG devices. From a more practical point of view, assuming a NIM operating around ~ 1.5 μm, the defect resonances that appear in the intrinsic gap region may be resolved with input pulses of temporal duration $\sim 50-100$ ps. Like metallic mirrors, NIM mirrors are limited by losses. NIMs that have already been fabricated appear to be somewhat lossy [1]. Nevertheless, NIM fabrication techniques are still in their infancy and developing fast. Finally, a NIM is a composite metallo-dielectric effective medium, and so it is reasonable to assume that its absorption will be somewhere between the absorption of the metal and that of the dielectrics. In our structure, increasing the level of absorption by a factor of 10 reduces the cavity field enhancement by approximately a factor of 4, and SH conversion efficiency by a factor of 18.

APPENDIX

Let us consider Eq. (2b) of the main text that here for the sake of clarity we write again

$$\frac{d^2}{dz^2}E_{2\omega}+\frac{(2\omega)^2\varepsilon_{2\omega}(z)\mu_{2\omega}(z)E_{2\omega}}{c^2}=-\frac{(2\omega)^2}{c^2}\mu_{2\omega}(z)d^{(2)}E_{\omega}^2(z). \tag{A1}$$

In the undepleted pump approximation E_ω is a known function and therefore the term at the right-hand side of Eq. (A1) acts as a source term. Because we are dealing with magnetic active materials, we associate to Eq. (A1) a Green function that satisfies the following equation:

$$\frac{\partial^2 G_\omega(z,\xi)}{\partial z^2}+\frac{(2\omega)^2\varepsilon_{2\omega}(z)\mu_{2\omega}(z)G_\omega(z,\xi)}{c^2}=\mu_{2\omega}(z)\delta(z-\xi), \tag{A2}$$

where $\delta(z-\xi)$ is the so-called "Dirac delta function" that is in this case multiplied by the z-dependent magnetic permeability of the structure. As we will see later in this section, this is a more convenient choice when, as in this case, the problem is related to stratifications of magnetically active media. We can write the formal solution of Eq. (A1) as follows:

$$E_{2\omega}(z)=-4\frac{\omega^2}{c^2}\int_0^L G_{2\omega}(\xi,z)d^{(2)}(\xi)E_\omega^2(\xi)d\xi. \tag{A3}$$

The Green function $G_{2\omega}(z,\xi)$ must be continuous at all points of the interval $0\leqslant z\leqslant L$ except at the point $z=\xi$, where it must have a jump equal to $\mu(z)$ in its first derivative. The calculation of the Green functions follows formally the same steps outlined in Ref. [17] with only two differences: (a) the jump in the derivative of the Green function at $z=\xi$ must be $\mu(z)$ and not 1 as would be the case for nonmagnetic material and (b) the boundary conditions appropriated for magnetic active materials must be applied. Following Ref. [17], Eq. (A2) can be solved in terms of the RTL and LTR propagating modes of the structure at frequency 2ω:

$$G_{2\omega}(z,\xi)=\begin{cases}\dfrac{1}{W}\Phi_{2\omega}^{(+)}(\xi)\Phi_{2\omega}^{(-)}(z), & 0\leqslant z<\xi,\\ \dfrac{1}{W}\Phi_{2\omega}^{(-)}(\xi)\Phi_{2\omega}^{(+)}(z), & L\geqslant z>\xi,\end{cases} \tag{A4}$$

where W is a conserved quantity, i.e., $dW/dz=0$, given by

$$W=W(\Phi_\omega^{(-)},\Phi_\omega^{(+)})\equiv\begin{vmatrix}\Phi_\omega^{(-)} & \Phi_\omega^{(+)}\\ \dfrac{1}{\mu}d\Phi_\omega^{(-)}/dz & \dfrac{1}{\mu}d\Phi_\omega^{(+)}/dz\end{vmatrix}.$$

Note that in the case of nonmagnetic materials, i.e., $\mu(z)=1$, W would be the Wronskian of the fundamental set of solutions. Now using the condition that W is a conserved quantity, it can be calculated using the boundary conditions at $z=L$ or $z=0$:

$$W=i\frac{n_{0,2}}{\mu_{0,2}}(2\omega)t_{2\omega}^{\mathrm{LTR}}=i\frac{n_{0,1}}{\mu_{0,1}}(2\omega)t_{2\omega}^{\mathrm{RTL}}, \tag{A5}$$

where $n_{0,1,2}$ and $\mu_{0,1,2}$ are the refractive index and the magnetic permeability of the materials surrounding the structure; $t_{2\omega}^{\mathrm{LTR}}$ and $t_{2\omega}^{\mathrm{RTL}}$ are, respectively, the linear transmission coefficient of the structure for an incident field from LTR and RTL, respectively.

[1] R. A. Shelby, D. R. Smith, and S. Schultz, Science **292**, 77 (2001).
[2] V. G. Veselago, Sov. Phys. Usp. **10**, 509 (1968).
[3] J. B. Pendry, Phys. Rev. Lett. **85**, 3966 (2000).
[4] R. W. Ziolkowski and E. Heyman, Phys. Rev. E **64**, 056625 (2001).
[5] R. W. Ziolkowski and A. D. Kipple, Phys. Rev. E **68**, 026615 (2003).
[6] G. D'Aguanno, N. Mattiucci, M. Scalora, and M. J. Bloemer, Laser Phys. **15**, 590 (2005).
[7] G. D'Aguanno, N. Mattiucci, M. Scalora, and M. J. Bloemer, Phys. Rev. E **71**, 046603 (2005).
[8] G. D'Aguanno, N. Mattiucci, M. Scalora, and M. J. Bloemer, Phys. Rev. Lett. **93**, 213902 (2004).
[9] G. D'Aguanno, N. Akozbek, N. Mattiucci, M. Scalora, M. J. Bloemer, and A. M. Zheltikov, Opt. Lett. **30**, 1998 (2005).
[10] Keunhan Park, Bong Jae Lee, Ceji Fu, and Zhuomin M. Zhang, J. Opt. Soc. Am. B **22**, 1016 (2005).
[11] D. R. Fredkin and A. Ron, Appl. Phys. Lett. **81**, 1753 (2002).
[12] Haitao Jiang, Hong Chen, Hongqiang Li, and Yewen Zhang Shiyao Zhu, Appl. Phys. Lett. **83**, 5386 (2003).
[13] D. Bria, B. Djafari-Rouhani, A. Akjouj, L. Dobrzynski, J. P. Vigneron, E. H. El Boudouti, and A. Nougaoui, Phys. Rev. E **69**, 066613 (2004).
[14] Michael W. Feise, Ilya V. Shadrivov, and Yuri S. Kivshar, Phys. Rev. E **71**, 037602-1 (2005).
[15] G. D'Aguanno, M. Centini, M. Scalora, C. Sibilia, M. Bertolotti, M. J. Bloemer, and C. M. Bowden, J. Opt. Soc. Am. B **19**, 2111 (2002).
[16] O. Di Stefano, S. Savasta, and R. Girlanda, J. Mod. Opt. **48**, 67 (2001).
[17] G. D'Aguanno, N. Mattiucci, M. Scalora, M. J. Bloemer, and A. M. Zheltikov, Phys. Rev. E **70**, 016612 (2004).
[18] J. Lekner, J. Opt. Soc. Am. A **11**, 2892 (1994).
[19] It is worth noting that an expression for SH conversion efficiency that involves overlap integrals has also been obtained in our Ref. [15] through a multiple scale expansion approach; see in particular Eqs. (16a) and (16b). While the two approaches give very similar results, in the case of Ref. [15] the formula for SH conversion efficiency also involves the calculation of the average of the momentum operator of the electromagnetic field that is coupled with the overlap integrals. There are two main advantages in using the Green's function approach instead of the multiple scale expansion approach to calculate SH conversion efficiency: (a) it does not relay on the existence of a fast and a slow scale of variation of the involved fields; (b) it only involves the calculation of overlap integrals and not that

of the momentum operator and therefore a much simpler expression can be obtained.

[20] A. Yariv and P. Yeh, *Optical Waves in Crystals* (John Wiley & Sons, New York, 1984).

[21] G. D'Aguanno, M. Centini, M. Scalora, C. Sibilia, M. Bertolotti, C. M. Bowden, and M. J. Bloemer, Phys. Rev. E **67**, 016606 (2003).

[22] J. Pendry, Opt. Photonics News **15**, 33 (2004).

[23] S. Linden, C. Enkrich, M. Wegener, J. Zhou, T. Koschny, and C. M. Soukoulis, Science **306**, 1351 (2004).

[24] V. A. Podolskiy, A. K. Sarychev, and V. M. Shalev, Opt. Express **11**, 735 (2003).